Torque Control of Induction Motors with Minimal Ripples Based on Continuous Control Set-MPC in a Wide Speed Range

Abdelsalam A. Ahmed[1], Byung Kwon Koh[2], and Young Il Lee[2], *Senior Member, IEEE*

[1] Department of Electrical Power and Machines Engineering, Faculty of Engineering, Tanta University, Tanta, Egypt
(e-mail: abdelsalam.abdelsalam@f-eng.tanta.edu.eg)

[2] Department of Electrical and Information Engineering, Seoul National University of Science and Technology, Seoul, Korea
(e-mail: yilee@seoultech.ac.kr)

Abstract—**This paper proposes a novel continuous control set model predictive control (CCS-MPC) method for torque control of induction motors (IMs). A systematic way to define a reference state for the given torque reference is provided. The reference state is determined according to the operational modes to yield the highest possible efficiency. Maximum torque per ampere (MTPA) operation is adopted considering Ohmic loss minimization below and above the base speed. MTPA in field-weakening region is adopted. In the proposed CCS-MPC, a cost index is defined using the derived reference state and the optimal control input is determined considering the input constraints. The proposed control method is implemented and validated by simulation and experimental studies. The results confirm that the proposed approach gives a very good dynamic performance overall speed with minimal torque and current ripples.**

***Index Terms*—Induction motors, torque control, field-weakening, continuous control set MPC.**

I. INTRODUCTION

In recent years, model predictive control (MPC) emerges as one of the most important advances in control of power electronics [1] [2]. There are mainly two types of MPC, finite control set MPC (FCS-MPC) and continuous control set MPC (CCS-MPC). The conventional FCS-MPC, with fixed duration period, has been applied for the induction motors (IM) [3] and for permanent magnet synchronous machines (PMSM) [4] [5]. A FCS-MPC was developed keeping the advantages of FCS–MPC with a fixed switching frequency in [6], [7]. The drawback of that MPC is that the time duration of the voltage vector is fixed, which limits the choice of the voltage vector in the inverter and produces large torque ripples and current oscillations. In order to avoid these drawbacks, some research activities have been conducted in [8] [9] with duration adjustment of the voltage vector.

The literature reports different maximum torque per ampere (MTPA) control methods for IM drives [10] [11] [12]. MTPA for IM concerning the flux-limited mode was presented in [13]. MTPA operation of an IM in the flux-weakening control (FWC) region was reported in [14]. In [9], MTPA control for IM drives was proposed in the form FCS-MPC including the operation in the flux-limited control (FLC) region. A reference state ensuring efficient operation of IM is derived for a given torque reference and the MPC formulation is made using this reference state. However the method of [9] does not cover the reference state when the speed exceeds the base value.

In this paper, the results of [9] are extended to cover field weakening region. A CCS-MPC formulation is adopted rather than FCS-MPC, in which the use of continuous but constrained control input is adopted. The computation of reference states considering MTPA production during the FWC is derived. To increase the efficiency on the drives system, ohmic loss minimization is considered. At low speed/torque values, flux-increased control (FIC) is used. If the controlled motor is requested to run at high speed at high torque, FLC technique is used to prevent saturation problems. When IM runs beyond base speed, the torque is maximized using FWC technique [14]-[16]. However, one contribution is the design of a complete CCS-MPC considering all of these issues. The main advantages of the proposed method with respect to conventional MPC [1] and FCS-MPC [8] [9] are that it is simple with low computational burden and yields fast torque responses with minimal ripples especially at high speeds while guaranteeing stability.

II. MODEL OF THE ELECTRICAL SYSTEM

The stator and rotor voltage equations of an IM in the synchronous reference frame are presented in [9]. The dynamic equations of IM can be described with state variable $x(t) = [i_{ds} \quad i_{qs} \quad \lambda_{dr} \quad \lambda_{qr}]^T$:

$$\dot{x}(t) = A_c(\omega_e(t))x(t) + B_c u(t). \tag{1}$$

The matrices A_c and B_c are

$$A_c(\omega_e) = \begin{bmatrix} -\frac{1}{\alpha}(R_s + \beta^2 R_r) + j\omega_e & \frac{\beta R_r}{\alpha L_r} + j\frac{\beta}{\alpha}\omega_r \\ \beta R_r & -\frac{R_r}{L_r} + j(\omega_e - \omega_r) \end{bmatrix}, B_c = \begin{bmatrix} \frac{1}{\alpha} & 0 \end{bmatrix}^T$$

where $j = \begin{bmatrix} 0 & -1 \\ 1 & 0 \end{bmatrix}$; R_s, R_r, L_s, L_r, L_m, ω_e, and ω_r denote stator resistance, rotor resistance, stator inductance, rotor inductance, mutual inductance, and rotational speeds of the stator current and rotor, respectively. $u(t) = [v_{ds} \quad v_{qs}]^T$ is the input vector, $\alpha = L_s - L_m^2/L_r$ is the stator transient inductance, and $\beta = L_m/L_r$ is the rotor coupling factor. It is worth while noting that the matrix A_c depends on the instantaneous value of mechanical speed ω_r. The discrete state space model of the IM is described using the Euler method with the sampling period T_s. The prediction of the stator current and rotor flux at the next sampling instant can be obtained as:

$$\begin{bmatrix} i_s[k+1] \\ \lambda_r[k+1] \end{bmatrix} = [A]\begin{bmatrix} i_s^* \\ \lambda_r^* \end{bmatrix} + [B]\begin{bmatrix} v_{ds}[k] \\ v_{qs}[k] \end{bmatrix} \tag{2}$$

978-1-5386-1317-7/17/$31.00 ©2017 IEEE

where $A = I_{4\times4} + A_c T_s$ and $B = B_c T_s$ are state space matrices [9]. Then, the electromagnetic torque of the IM in terms of the stator current, rotor flux and number of poles P is given as:

$$T_e = \frac{3}{2}\frac{P}{2}\frac{L_m}{L_r}\left(\lambda_{dr} i_{qs} - \lambda_{qr} i_{ds}\right) \quad (3)$$

The control input u[k] is generated by a 2-level VSI using the SV-PWM. Then, it can be considered as a continuous signal constrained as follows [14].

$$\sqrt{u[k]^T u[k]} = \|u[k]\| \le \frac{V_{dc}}{\sqrt{3}}, \quad (4)$$

where V_{dc} represent the DC-link voltage of the inverter. Fig. 1 describes the electric system for control and drive of the IM.

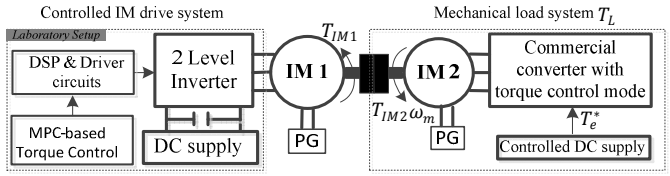

Fig. 1. IM drive system

III. PROPOSED CCS-MPC TORQUE CONTROL

A. Computation of the Reference State for a Given Torque

In this section, we introduce how to determine a reference state for torque control to guarantee the most efficient operation while following the given torque reference $T_e^*(k)$. In IM, the rotor flux rotates at the synchronized speed ω_e and the rotational angle θ_e changes accordingly. Considering the principle of indirect FOC [9], the electrical reference state $x^*(T_e^*(k))$ can be defined as follows:

$$\begin{aligned} x^*(T_e^*, \lambda^*) &= [i_{ds}^* \quad i_{qs}^* \quad \lambda_{dr}^* \quad \lambda_{qr}^*]^T \\ &= \left[\frac{\lambda^*}{L_m} \quad \frac{2}{3}\frac{2}{P}\frac{L_r}{L_m}\frac{T_e^*}{\lambda^*} \quad \lambda^* \quad 0\right]^T \end{aligned} \quad (5)$$

The rotor flux reference λ^* in (5) could be determined according to operational region; i.e. FIC, FLC, and FWC. Calculation of λ^* has been presented in [9] for the regions below the base speed; i.e. FIC and FLC. However, in this paper, minimization of stator and rotor ohmic losses is adopted below the base speed [17]. Moreover, calculation of λ^* is presented here in FWC region.

B. Flux Reference in Field-weakening Region

In FWC, the reference torque should be modified according to the maximum available torque which in turn depends on the driving speed. In IM drives, FWC is readily achieved by reducing the direct axis current component i_{ds}^e and manipulating the quadrature current i_{qs}^e according to a chosen control strategy. With intensive mathematical derivation, considering the stator resistance R_s for more accuracy, the ellipse's equation of the voltage inequality as

$$i_{ds}{}^2 + \sigma^2 i_{qs}{}^2 \le \left(\frac{V_{smax} - I_{smax} * R_s}{L_s\, \omega_e}\right)^2 \quad (6)$$

where $I_{smax}^2 = i_{ds}{}^2 + i_{qs}{}^2$ and σ is the total leakage factor $\sigma = 1 - L_m^2 / L_s\, L_r$. On the other hand, in FWC region, the current components i_{ds} and i_{qs} should satisfy the circle

$$i_{ds}{}^2 + i_{qs}{}^2 \le I_{smax}^2, \quad (7)$$

In the FWC, the reference state of (5) can be determined from the intersection of the current-limit circle and the voltage-limit ellipse at a given operating frequency using (6) and (7) as follows:

$$i_{ds}{}^* = \sqrt{\frac{((V_{smax} - I_{smax} * R_s)/\omega_e)^2 - (\alpha\, I_{smax})^2}{L_s^2 - \alpha^2}} \quad (8)$$

Then, $i_{qs}{}^* = \sqrt{I_{smax}^2 - i_{ds}{}^{*2}}$, $\lambda_{dr}{}^* = L_m\, i_{ds}{}^*$ and $\lambda_{qr}{}^* = 0$. It can be noticed that $i_{ds}{}^*$ depends on ω_e regardless of the torque reference T_e^* whereas $i_{qs}{}^*$ depends on T_e^*. From the reference torque of (5), the maximum allowable torque can be defined as

$$T_{e\_max}^* = \frac{3}{2}\frac{P}{2}\frac{L_m^2}{L_r}\, i_{ds}{}^*\, i_{qs}{}^* \quad (9)$$

Here, the current $i_{ds}{}^*$ calculated from (8) is used for all torque values at one particular speed. When the torque is controlled in the FWC region, the reference torque T_e^* should be bounded by $T_{e\_max}^*$ of (9) i.e. the modified reference torque T_{efw}^* is stated as:

$$T_{efw}^* = \begin{cases} T_e^* & \text{if} \quad T_e^* \le T_{e\_max}^* \\ T_{e\_max}^* & \text{if} \quad T_e^* > T_{e\_max}^* \end{cases} \quad (10)$$

where the slip speed and the corresponding synchronous speed are calculated as $\omega_{sl}^* = \frac{1}{\tau_r}\frac{i_{qs}{}^*}{i_{ds}{}^*}$; where $\omega_e = \omega_{sl}^* + \omega_r$.

C. CCS-MPC Design

For the given reference state x^*, a state tracking problem can be formulated as

$$\lim_{k\to\infty} x(k) = x^*, \ \ subject\ to\ (2)\ and\ (4) \quad (11)$$

This section presents MPC method for the discrete-time system (2) to solve the state tracking problem of (11) by minimizing a cost index without any use of numerical methods. For this purpose, a one-step ahead predicted error state $e_x[k+1|k]$ can be defined as

$$e_x[k+1|k] = x^* - x[k+1|k] = x^* - (A\, x[k] + B\, u[k]) \quad (12)$$

Using the foregoing error prediction (12) and based on the reference state $x^*(T_e^*, \lambda^*)$ of (5), the cost index for the proposed control system is defined as

$$J(k) = (x^*(T_e^*, \lambda^*) - x[k+1|k])^T W (x^*(T_e^*, \lambda^*) - x[k+1|k]) \quad (13)$$

The W is a positive definite weighting matrix and $x[k+1|k]$ is the prediction of $x[k+1]$ based on the available data at time k. Note that this cost penalizes the predicted state error at the next time step. The choice of the weighting matrix W is important to obtain a good state tracking performance and stability. An optimization technique based on linear matrix inequality (LMI) method can be used for determining the optimal W.

We now consider the input constrained optimization problem associated with $J\big(x(k),u(k)\big)$

$$\min_{u(k)} J\big(x(k),u(k)\big) \text{ subject to (2) and (4)} \tag{14}$$

The control $u(k)$ in (2) and (12) is supposed to be applied to the inverter at time step k to minimize the cost index $J(k)$ (13) concerning the predicted state tracking errors at time step $(k+1)$. In real applications, however, there is a time delay due to the computation time and modulation mechanism i.e. the control input computed at time step k is actually applied to the inverter at time step $(k+1)$. This time delay may degrade the performance, and we need to compensate for it. From (2), the prediction $x[k+2|k]$ can be made as:

$$x[k+2|k] = Ax[k+1|k] + Bu[k] \tag{15}$$

Based on observation of (15), the cost index (13) is modified as follows:

$$J(k) = (x^*(T_e^*,\lambda^*) - x[k+2|k])^T W (x^*(T_e^*,\lambda^*) - x[k+2|k]) \tag{16}$$

The reference states derived in (5) may not be correct because of uncertainties, which lead to a steady state tracking error. In order to prevent the steady state tracking error, these state references are compensated by integrating the tracking error:

$$x_s^*[k] = x^*(T_e^*,\lambda^*) + K_s e_s[k] \tag{17}$$

where tracking error $e_s[k] = e_s[k-1] + (x^*(T_e^*,\lambda^*) - x[k])$ with a proper gain K_s. This compensated reference state $x_s^*[k]$ substitutes for reference state of the cost index (16) to yield (18).

$$J(k) = (x_s^*[k] - x[k+2|k])^T W (x_s^*[k] - x[k+2|k]) \tag{18}$$

In order to derive the optimizer of the optimization problem (14) explicitly, the cost index (18) is rewritten in terms of the control input $u[k]$ with the help of (15) as:

$$J(k) = \big(x_s^*[k] - (Ax[k+1|k] + Bu[k])\big)^T W (x_s^*[k] - (Ax[k+1|k] + Bu[k])) \tag{19}$$

Let $u_{uc}^*(k)$ be the unconstrained optimizer of $J(k)$ in (19). Then, $u_{uc}^*(k)$ can be obtained by solving $\frac{\partial J(x(k),u(k))}{\partial u(k)} = 0$ to give:

$$u_{uc}^*(k) = (B^T W B)^{-1}\big(B^T W (x_s^*(T_e^*,\lambda^*) - \mathrm{A}\, x[k+1|k])\big) \tag{20}$$

It is apparent that the optimizer $u_c^*(k)$ of the optimization problem in (20) is the same as the unconstraint $u_{uc}^*(k)$ if it is within the limit i.e. $\|u_{uc}^*(k)\| \le V_{smax}$, as shown in Fig. 2(a).

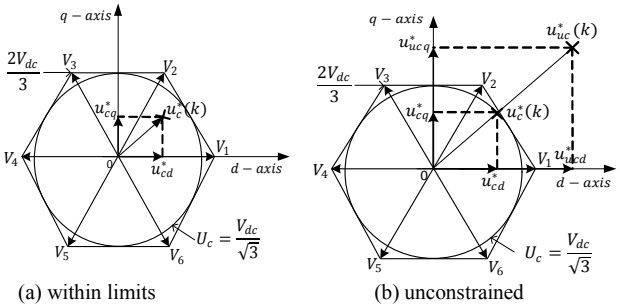

(a) within limits (b) unconstrained

Fig. 2. Input control voltages

We now consider the case in which $\|u_{uc}^*(k)\| > V_{smax}$. Note that the feasible set of inputs satisfying (4) can be represented as a circle in the d-q axis as given in Fig. 2. Assuming that W is chosen so that

$$B^T W B = I \tag{21}$$

is satisfied, then the level sets of control voltage at all values of the cost function are circles. In this case it is clear that $u_c^*(k)$ is at the tangential point of the boundary of the circle with the level set of $J(k)$, see Fig. 2(b). Then, the chosen set point of $u_c^*(k)$ is determined by finding the intersection point of the boundary of the feasible input region with the line segment from the point $u(k) = 0$ to $u_{uc}^*(k)$, [18]. Therefore, the MPC algorithm $u_c^*(k)$ is established by

$$u_c^*(k) = \begin{cases} u_{uc}^*(k) \quad (\text{of } (40)) & \text{if } \|u_c^*[k]\| \le V_{smax} \\ \dfrac{V_{smax}}{\|u_c^*[k]\|} u_{uc}^*(k) & \text{if } \|u_c^*[k]\| > V_{smax} \end{cases} \tag{22}$$

The proposed control system based on CCS-MPC is described in Fig.3.

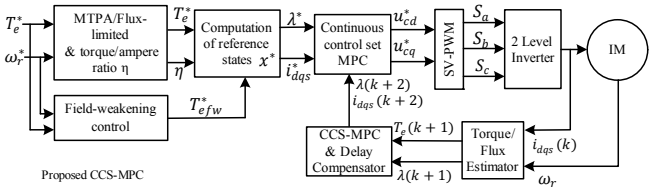

Fig. 3. The configuration of the proposed CCS-MPC torque control of IM

Table I: IM parameters

DC-bus volt [V]	V_{dc}	450
Number of Poles	P	4
Power factor	$\cos\theta$	0.875
Rated voltage [V]	Y/Δ	220/380
Rated current [A]		14.2/8.2
Stator Resistance [Ω]	R_s	1.77
Rotor Resistance [Ω]	R_r	1.275
Stator Inductance [H]	L_s	0.157
Rotor Inductance [H]	L_r	0.158
Mutual Inductance [H]	L_m	0.15
Inertia coefficient [Kg.m^2]	J	0.0056
Rated Motor Speed [rpm]	ω_N	1740
Rated Motor Frequency [Hz]	f_N	60
Rated Power [kW]	P_N	3.7

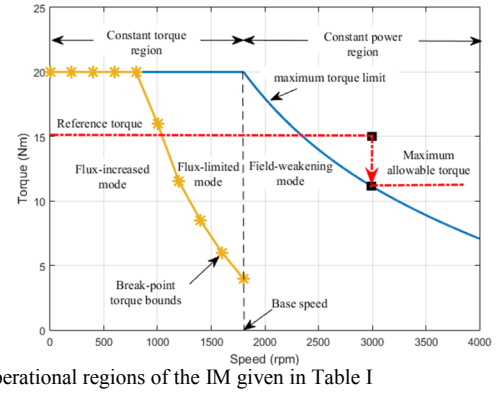

Fig. 4. Operational regions of the IM given in Table I

IV. SIMULATION RESULTS

In Fig. 4, the overall speed rage is divided into three regions. At low speed, the flux is increased as the reference torque T_e^* increases. Then the flux-limited region is followed. The break-point torque bounds between these two regions is determined off-line and saved as a Look-up table to be used in the on-line implementation process. Also, the FWC is adopted beyond the base speed of 1740 rpm.

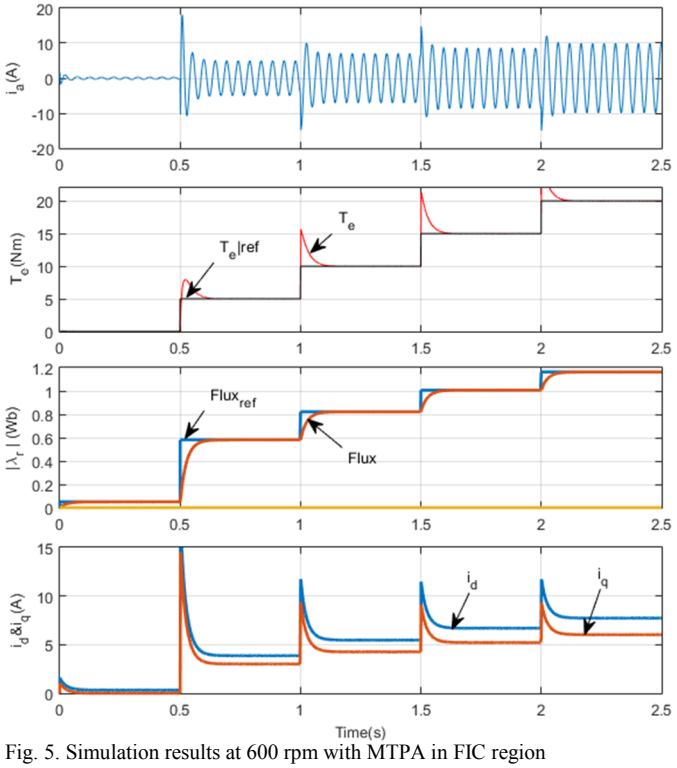

Fig. 5. Simulation results at 600 rpm with MTPA in FIC region

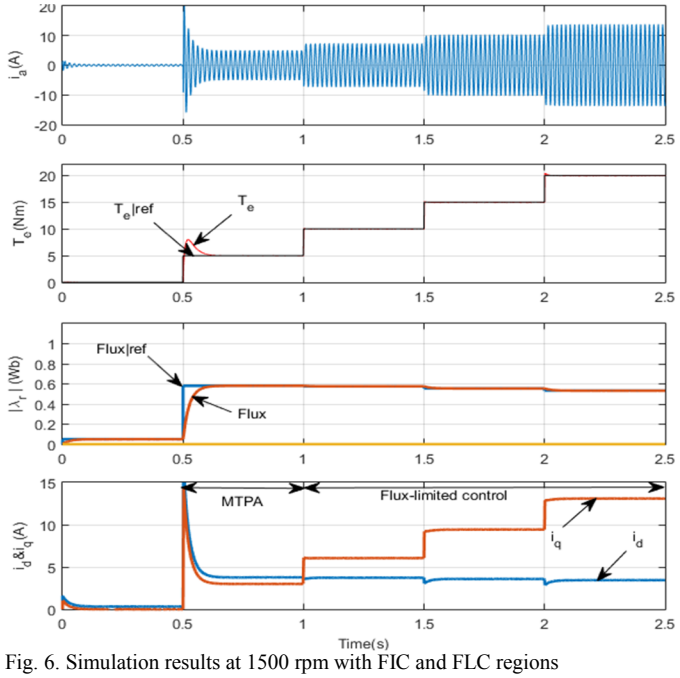

Fig. 6. Simulation results at 1500 rpm with FIC and FLC regions

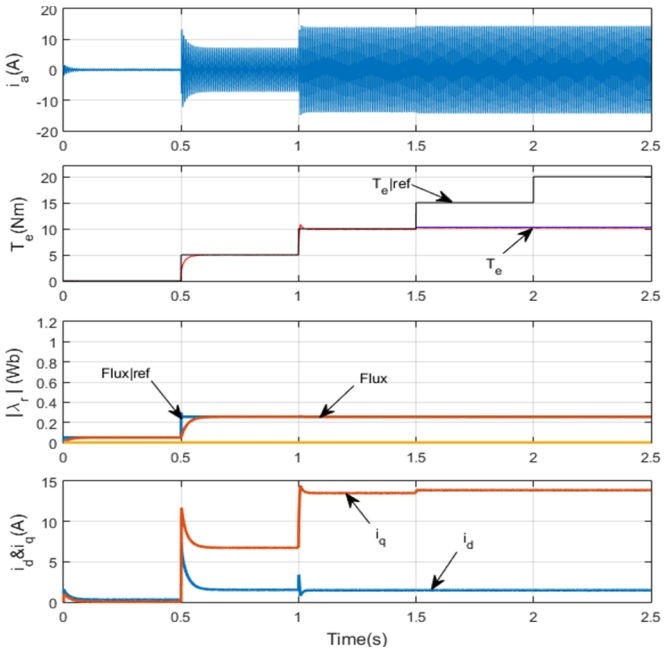

Fig. 7. Simulation results at 3000 rpm with MTPA in FWC region

When the IM is tested at speed of 3000 rpm at a given $T_e^* = 15\ Nm$ and the rated current for the star connected load remains at 14.2 A while the maximum voltage is set as 450 Vdc according to FWC algorithm, the flux is weakened and the reference torque is modified to the maximum allowable torque of 10.5 Nm according to (9). The parameters of IM and the controller are defined in Table I.

A. Dynamic Performances with Change of Torque Reference

The performance of the controlled IM with the proposed CCS-MPC below and above base speed is investigated with change of reference torque in simulation. During this dynamic process, torque, phase current, rotor flux, and d-q currents are observed. The results at 600, 1500 and 3000 rpm are depicted in Figs. 5, 6 and 7, respectively.

Fig. 5 shows the results at low speed of 600 rpm with MTPA. It can be noticed that the ratio between the current components are equal to the factor $K_{MTPA} = 1.282$ that assures the MTPA. Rotor flux is noticed to be increased as the torque increases.

When the input torque is higher than the boundary of break-point torque, defined via the look-up table, the IM is controlled in FLC to prevent the saturation of magnetic circuit. The transition from FIC to FLC is shown in Fig. 6 at speed of 1500 rpm. At time of 1S, the flux is limited approximately to 0.6 Web.

When the IM is driven at 3000 rpm, the proposed CCS-MPC with FWC is applied as seen in Fig.7. It can be noticed that the torque is matched to its reference at 5 and 10 Nm; whereas the reference torque is modified to 10 Nm at time of 1.5 sec according to (9). Also, it is observed that the rotor flux is decreased to 0.25 Web. Observation of d-q currents shows that the d-axis current is fixed at the optimal value of (8); whereas q-axis current is increased in steps following the change in torque (8).

V. EXPERIMENTS

A. Experimental setup

To verify the performance of the proposed control system, an experimental setup has been established as shown in Fig. 8. The setup used for experimental validation of the proposed method consists of 3.7kW IM driven by a 5.6 kW VSI with its interface circuits. The experiments are occurred at constant speeds using 5.5 kW IM driven by a 5.5 kW commercial inverter with vector control. The experimental setup incorporates a control board, which is based on the 32-bit floating point TMS320F28335 DSP. The current was measured directly using a current probe, but the torque and flux responses computed by the embedded controller were transferred to D/A converters and measured by an oscilloscope. The control method is implemented with sampling frequency of 10 kHz. To test the performance of the IM with the proposed method for torque control, a drive motor is driven at a fixed speed using a commercial converter with vector control. Then, the IM under control is used as a controlled load by applying a reference torque with different levels. Finally, the performance of the IM is studied.

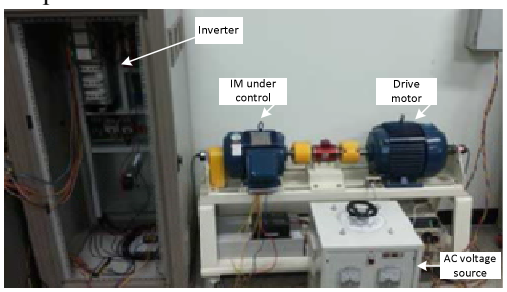

Fig. 8. Setup of MG-Set and 2L-VSI for the experiment

B. Dynamic Performance with Change in Torque Reference

The performances of the proposed CCS-MPC method are investigated at different speeds in experiment. Figs. 9, 10 and 11 show the experimental results at different torque levels of 0, 5, 10, 15, and 20Nm, while the motor runs at 600, 1500 and 3000rpm, respectively. Experimental results shown in Fig. 9 are matched to the simulation results shown in Fig. 5 when the motor runs at 600 rpm with MTPA control in FIC region. The pictures depict the performance at different torque levels of 0, 5, 10, 15, and 20 Nm and at speed of 600 rpm. In this test, the phase current increases in steps as the torque. Rotor flux is increased in steps with torque. Below the break-point torque bounds, shown in Fig. 4, FIC is applied at 5Nm@1500rpm, as shown in Fig 10. When the torque reference exceeds the break-point torque, the IM is controlled in FLC. The transition from flux-increased mode to flux-limited mode can be noticed at 1500 rpm as shown in Fig. 10 at time of 3.6 S. The torque follows its reference well. Flux is increased with MTPA control at 5Nm; then it is fixed approximately at 0.6 Web. The phase current is increased in steps as the torque is increased. The d-axis current is fixed at 4 A following the limited flux; whereas q-axis current is increased following step increase of torque to read 12A at 20Nm. Also, the experimental results in Fig.10 coincide with the simulation results in Fig.6.

The performances of the proposed CCS-MPC with FWC are shown in Fig. 11 at 3000 rpm. These figures show the input reference torque and modified reference torque and the estimated torque of (6). All torques are matched at the torque levels of 5, 10, and 15 Nm at 2100 rpm, not shown in this manuscript; whereas the torques are matched at the levels of 5 and 10 Nm at 3000 rpm. The reference torque is constrained to 10 Nm at 3000 rpm, while at 2100 rpm, the reference torque is constrained to 17 Nm. In addition, it can be observed that the q-axis and phase current waves are increased in steps following torque steps; whereas the flux is approximately fixed at a weakened value of 0.4 and 0.25 Web at 2100 and 3000 rpm, respectively. All these experimental results are similar to that shown in simulation results in Fig. 7.

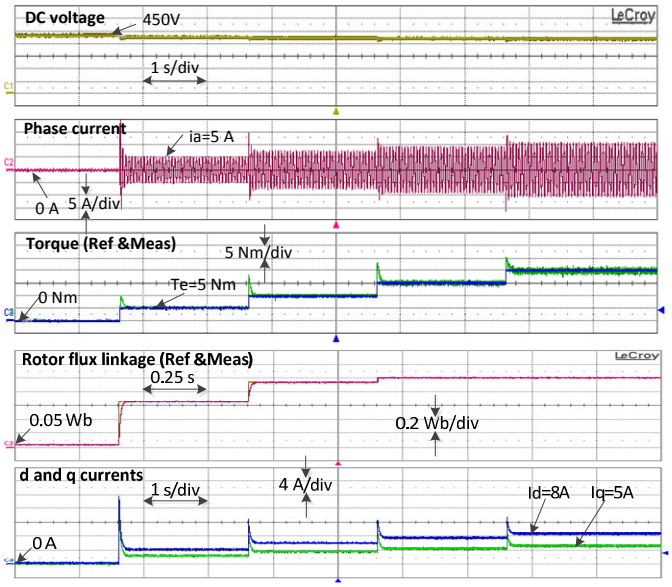

Fig.9. Experimental results at 600 rpm with MTPA control in FIC region: from top to bottom: DC link voltage [100V/div], phase current [5A/div], developed torque [5Nm/div], rotor flux [0.2Web/div], d-q currents [4A/div], and time scale is [1 S/div].

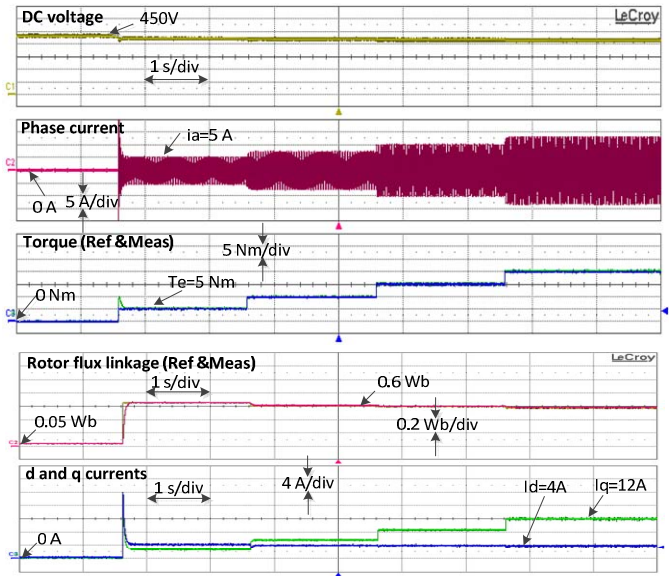

Fig.10. Experimental results at 1500 rpm with FLC: from top to bottom: DC link voltage [100V/div], phase current [5A/div], developed torque [5Nm/div], rotor flux [0.2Web/div], d-q currents [4A/div], and time scale is [1 S/div].

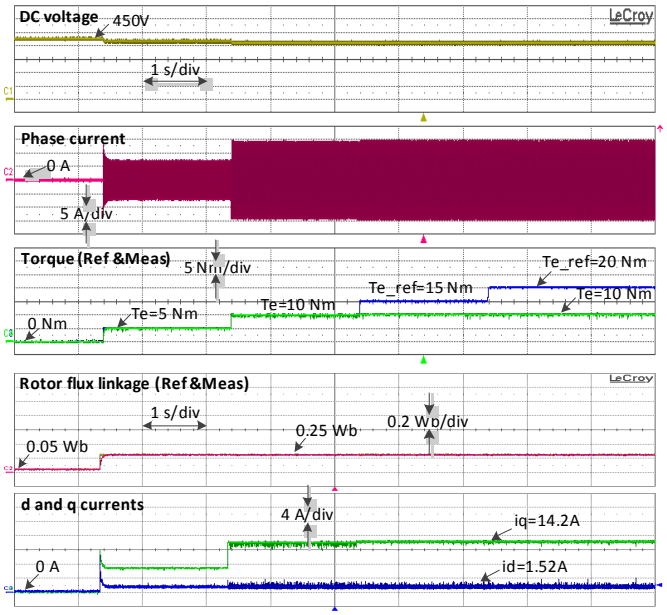

Fig.11. Experimental results at 3000 rpm with FWC, from top to bottom: DC link voltage [100V/div], phase current [5A/div], developed torque [5Nm/div], rotor flux [0.2Web/div], d-q currents [4A/div], and time scale is [1S/div].

C. *Steady State Performance*

Figure 12 shows the experimental steady-state results at 3000 rpm. The reference torque was set to be the rated value of 20 Nm. It is seen that and proposed MPC presents much lower torque ripple than that of FCS-MPC presented in [9]. From a close observation, it can be noticed that the torque is limited to 10 Nm which is considered the maximum allowable torque at that speed, see (10).

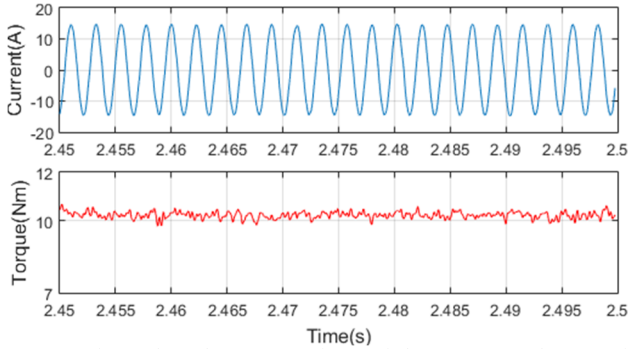

Fig.12. Experimental steady-state waveforms of phase current and torque of the IM for proposed CCS-MPC at 3000 rpm with FWC control.

VI. Conclusion

The proposed CCS-MPC presents a good dynamic performance at different operating conditions. Moreover, the ripples of torque and current waves have notably been minimized. Torque response is very fast without overshoot except when MTPA technique is applied because of coupling between torque and field current components. Control of rotor flux of the IM is precisely achieved to get the required torque respecting the voltage and current constraints in three regions, FIC, FLC, and FWC. Therefore, during experiment, the IM has been controlled without problems of saturation and overload. Maximization of the torque per ampere in the three tested regions increases the efficiency of the drive system. Robustness against step torque response is achieved. Similarity of the experimental and simulation results verify the implementation.

References

[1] P. Cortes, M. Kazmierkowski, R. Kennel, D. Quevedo, and J. Rodriguez, "Predictive control in power electronics and drives," IEEE Trans. Ind. Electron., vol. 55, no. 12, pp. 4312–4324, Dec. 2008.

[2] J. Rodriguez and P. Cortes, "Predictive Control of Power Converters and Electrical Drives", Hoboken, NJ, USA: Wiley, 2012.

[3] F. Wang, S. Li, X. Mei, W. Xie, J. Rodríguez, and R. M. Kennel, "Model-based predictive direct control strategies for electrical drives: An experimental evaluation of PTC and PCC methods", IEEE Trans. Ind. Informatics, vol. 11, no. 3, June 2015.

[4] E. Fuentes, J. Rodriguez, C. Silva, S. Diaz, and D. Quevedo, "Speed control of a permanent magnet synchronous motor using predictive current control," in IEEE 6th International Power Electronics and Motion Control Conference, IPEMC '09, pp. 390–395, May 2009.

[5] A. A. Ahmed, "Fast-speed drives for permanent magnet synchronous motor based on model predictive control", IEEE Vehicle Power and Propulsion Conference (VPPC), Montreal, Canada, 2015.

[6] S. Saeidi, R. Kennel, "A novel algorithm for model predictive control of ac electric drives", 2nd International Electric Drives Production Conference (EDPC), 2012.

[7] S. Saeidi and R. Kennel, "Continuous set nonlinear model predictive control for an induction motor", 15th European Conference on Power Electronics and Applications (EPE), 2013.

[8] Y. Zhang, and H. Yang, "Model predictive torque control of induction motor drives with optimal duty cycle control", IEEE Trans. Power Electronics, vol. 29, no. 12, pp. 6593-6603, 2014.

[9] A. A. Ahmed, B. K. Koh, H. S. Park, K.B. Lee, and Y. I. Lee, "Finite Control Set Model Predictive Control Method for Torque Control of Induction Motors using a State Tracking Cost Index", IEEE Transactions on Industrial Electronics, to appear.

[10] R. Bojoi, Z. Li, S. A. Odhano, G. Griva and A. Tenconi, "Unified direct-flux vector control of induction motor drives with maximum torque per ampere operation", IEEE Energy Conversion Congress and Exposition (ECCE), 2013.

[11] C. Kwon and S. D. Sudhoff, "An improved maximum torque per amp control strategy for induction machine drives" Conf. Rec. IEEE Applied Power Electronics Conference and Exposition (APEC), 2005, 6, vol. 2, pp. 740–745.

[12] S. Dymko, S. Peresada, R. Leidhold, "Torque control of saturated induction motors with torque per ampere ratio maximization", IEEE Intern. Conf. on Intelligent Energy and Power Systems, 2014.

[13] O. Wasynczuk, S. D. Sudhoff , K. A. Corzine, Jerry L. Tichenor, P. C. Krause, I. G. Hamen, L. M. Taylor, "A maximum torque per ampere control strategy for induction motor drives", IEEE Trans. Energy Conversion, vol. 13, no. 2, June 1998.

[14] M. Preindl and S. Bolognani, "Model predictive direct torque control with finite control set for PMSM drive systems, Part 1: Maximum torque per ampere operation", IEEE Trans. Indus. Informatics, vol. 9, no. 4, Nov. 2013.

[15] S. H. Kim, and S. K. Sul, "Maximum torque control of an induction machine in the field weakening region", IEEE Trans. Indus. Applic., vol. 31, no. 4, Jul./Aug. 1995, pp 787-794.

[16] J. K. Seok, and S. K. Sul, "Optimal flux selection of an induction machine for maximum torque operation in flux-weakening region", IEEE trans. power electr., vol. 14, no. 4, Jul.1999, pp 700-708.

[17] R. Marino, P. Tomei, and C. M. Verrelli, "Induction Motor Control Design", Springer-Verlag London Limited, Ch.1, "Steady-state Operating Conditions with Sinusoidal Voltages", P.P. 19-20, 2010.

[18] S. K. Kim, H. S. Park, and Y. I. Lee, "Stabilizing model predictive control for torque control of permanent magnet synchronous motor", IEEE Trans. Con. Systems Tech., vol. 11, no. 4, Dec. 2013.